Article

Influence of Alloying Treatment and Rapid Solidification on the Degradation Behavior and Mechanical Properties of Mg

Jian Chen [1],[†], Ping Wu [2],[†], Qiyuan Wang [1], Youwen Yang [3], Shuping Peng [4],[5],[6], Yuanzhuo Zhou [3], Cijun Shuai [3],* and Youwen Deng [1],*

[1] Department of Emergency Medicine, The Second Xiangya Hospital, Central South University, Changsha 410083, China; yjcj0821@csu.edu.cn (J.C.); idletwo@gmail.com (Q.W.)

[2] College of Chemistry, Xiangtan University, Xiangtan 411105, China; pingwu@xtu.edu.cn

[3] State Key Laboratory of High Performance Complex Manufacturing, the State Key Laboratory for Powder Metallurgy, Central South University, Changsha 410083, China; yangyouwen@csu.edu.cn (Y.Y.); zyz420357155@csu.edu.cn (Y.Z.)

[4] The Key Laboratory of Carcinogenesis of the Chinese Ministry of Health, Xiangya Hospital, Central South University, Changsha 410008, China; shuping@csu.edu.cn

[5] The Key Laboratory of Carcinogenesis and Cancer Invasion of the Chinese Ministry of Education, Cancer Research Institute, Central South University, Changsha 410078, China

[6] Hunan Key Laboratory of Nonresolving Inflammation and Cancer, Disease Genome Research Center, The Third Xiangya Hospital, Central South University, Changsha 410078, China

* Correspondence: shuai@csu.edu.cn (C.S.); drywdeng@csu.edu.cn (Y.D.);
   Tel.: +86-731-8480-5412 (C.S.); +86-731-8529-2120 (Y.D.)

† These authors contributed equally to this work.

Abstract: Magnesium (Mg) has drawn increasing attention as a tissue engineering material. However, there have been very few studies of laser-melted Mg-Zn alloys. In this study, four binary Mg-xZn (x = 2, 4, 6 and 8 wt. %) alloys were fabricated by laser melting. The influence of zinc (Zn) content and technique on the degradation behavior and mechanical properties of Mg were discussed. Results revealed that Mg-xZn alloys consisted of an α-Mg matrix and MgZn phases, which dispersed at the grain boundaries. In addition, the MgZn phase increased with the increase in Zn content. The laser-melted alloy had fine homogenous grains, with an average grain size of approximately 15 μm. Grain growth was effectively inhibited due to the precipitation of the MgZn phase and rapid solidification. Grain refinement consequently slowed down the degradation rate, with Zn content increasing to 6 wt. %. However, a further increase of Zn content accelerated the degradation rate due to the galvanic couple effect between α-Mg and MgZn. Moreover, the mechanical properties were improved due to the grain refinement and reinforcement of the MgZn phase.

Keywords: Mg-Zn alloys; alloying treatment; laser melting; degradation behavior; grain refinement

1. Introduction

Magnesium (Mg), as a promising biomaterial, has attracted much attention due to its natural biodegradability and favorable cytocompatibility [1,2]. Moreover, it plays essential roles in human metabolism, cellular structure and function, and bone growth [3–5]. However, the degradation rate of Mg becomes excessively fast in a physiological environment, resulting in quick loss of mechanical strength [6]. Meanwhile, the released hydrogen gas during the fast degradation process will accumulate in the body, leading to undesirable subcutaneous emphysema [7].

Alloying treatment is an effective method to improve the degradation behavior and mechanical properties of Mg. Many kinds of alloying elements have been studied including Zn, manganese (Mn) and aluminum (Al) [8–10]. Among these elements, Zn has great application prospects, since it is an essential trace element in a physiological environment, and can participate in bone metabolism and growth [11]. Boehlert et al. investigated the mechanical performance of as-cast Mg-Zn alloys by controlling the Zn content, finding that the tensile strength was enhanced from 62 MPa to 114 MPa [12]. Zhang et al. [13] studied the degradation behavior of extruded Mg-Zn alloys, suggesting that Zn could effectively reduce the degradation rate of Mg in simulated body fluid (SBF).

However, Mg alloys prepared by traditional preparation processes, such as casting and powder metallurgy, exhibit coarsened grains and non-homogeneous microstructure, resulting in inadequate mechanical properties and poor degradation behavior [14]. Laser melting, as a typical rapid solidification technology, has an extreme high cooling rate, which is above 10^5 K/s [15]. In addition, such a rapid solidification effectively inhibited the grain growth, forming a homogeneous, finer crystalline structure [16]. Moreover, the rapid solidification will also increase the solid solubility of alloying elements, which is helpful in forming a protective film on the surface of the Mg alloy, and improve the degradation behavior [17,18]. Thus, laser melting exhibited great superiority and the potential to enhance Mg properties.

To the best of our knowledge, limited reports on the microstructure, degradation behavior and mechanical properties of Mg-Zn alloys fabricated by laser melting have been published. In this work, both alloying Zn and rapid solidification were employed to improve Mg properties. The processing parameters, such as scanning speed, laser power, layer thickness and spot diameter, were obtained through laser melting experiments. The effects of Zn content and technique on Mg-Zn alloys were analyzed using a scanning electron microscope (SEM), an optimal optical microscopy, X-ray diffraction (XRD), immersion test, and indentation test.

2. Materials and Methods

2.1. Materials

Original materials including the Mg powder (Figure 1a) and Zn powder (Figure 1b) were both purchased from Shanghai Naiou Nano Technology Co., Shanghai, China. The powders were blended with different Zn content (2, 4, 6, and 8 wt. %) by ball milling (DECO-PBM-V-0.4L.DECODK CO., Changsha, China) at 300 rpm for 4 h. The mixed powders after ball milling and before melting were shown in Figure 1c. The process was performed under a mixed gas atmosphere of SF_6 (0.3 vol. %) and CO_2 (Bal.).
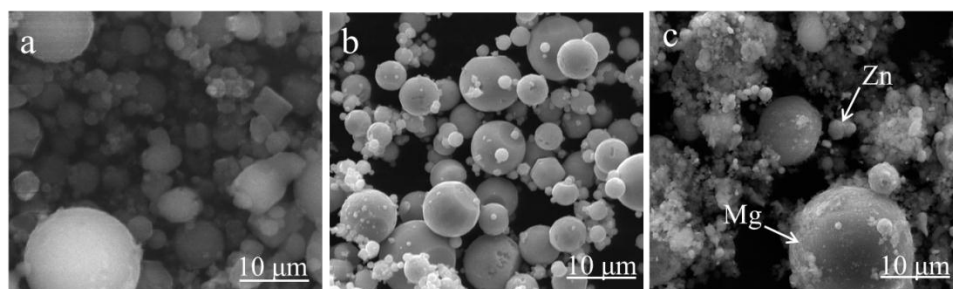

Figure 1. The original powder: (**a**) Mg; (**b**) Zn; and (**c**) mixed powder.

2.2. Methods

Mg-*x*Zn alloys were prepared using a home-made laser melting system, which consisted of a laser focusing system, a three-dimension motion platform, and a computer control system [19]. First, a thin layer of powder was paved on the substrate, and the laser beam scanned the powder layer basing on the computer control system. As one layer was deposited, the substrate descended by one layer

of thickness. All procedures occurred in an argon environment to prohibit oxidation. The detailed experiment parameters were shown in Table 1.

Table 1. Experiment parameters.

Laser Power (W)	Laser Scan Speed (mm/s)	Layer Thickness (mm)	Spot Diameter (μm)
70	100	0.1–0.2	50

2.3. Microstructures Characterization

The samples were successively polished with different grit SiC sandpapers (500, 1000, and 2000 grit). Then, the crystalline size was studied by optical microscopy (PMG3; Olympus Corporation, Tokyo, Japan) after being etched with picral solution (4.2 g of picric acid, 70 mL of ethanol, 10 mL of ethylic acid and 10 mL of distilled water). The distribution of the second phase was studied by scanning electron microscopy (SEM, JSM-5600LV, JEOL Co., Tokyo, Japan) combined with energy-dispersive spectroscopy (EDS, JSM-5910LV JEOL Co., Tokyo, Japan).

After immersion in simulated body fluid (SBF), all Mg-Zn alloys and corrosion products were studied using the XRD (D8-Advance; German Bruker Co., Karlsruhe, Germany). Analysis conditions were: voltage, 40 kV; electric current, 250 mA. Scanning velocity was $6°·min^{-1}$ with 2θ ranging from $10°$ to $80°$.

2.4. Immersion Tests

Hydrogen evolution measurements were performed to evaluate the degradation behavior of the Mg-Zn alloy. SBF acted as the degradation medium, including: 0.06 g/L of Na_2HPO_4, 0.06 g/L of KH_2PO_4, 0.2 g/L of $MgSO_4·7H_2O$, 0.14 g/L of $CaCl_2$, 0.4 g/L of KCl, 0.35 g/L of $NaHCO_3$ and 6.0 g/L of NaCl. The temperature was maintained at $37 ± 0.5 °C$. The Mg-Zn alloys ($5 × 5 × 3$ mm^3) were immersed in 250 mL SBF solution. The evolved hydrogen was collected into a burette through a funnel mounted over the alloys. The Mg-Zn alloy was immersed in SBF for three days, ultrasonically vibrated in ethyl alcohol for 20 min, dried in air, and observed by SEM.

2.5. Mechanical Properties

Indentation tests were carried out using an HXD digital hardness tester (Taiming Optical Instrument Corporation, Shanghai, China) equipped with a square-based pyramid-shaped diamond indenter and an incident light microscope (Taiming Optical Instrument Corporation, Shanghai, China). Before indentation, the alloys were inset in epoxy using a pointing machine (XQ-2B, Contract Optical Instrument Corporation, Shanghai, China), grinded smooth on 1000 grit SiC sandpaper, and then polished using the JP06A single-axle grinding polisher (Xibin Opto-Electronic Equipment Company, Wuxi, China). Finally, the diamond indenter was pressed into the alloys with a load of 0.98 N and kept for 15 s. For each measurement, 10 separated points of indentations were performed; and the mean length of two catercorners was calculated. The hardness value could be calculated by [20]:

$$Hv = 0.1891F/D^2 \tag{1}$$

where F was the pressing force, D was the arithmetic mean of two gauged catercorners, and Hv was the value of Vickers hardness. All experimental data were calculated as means ± standard deviation.

3. Results and Discussion

3.1. Microstructures

The crystalline characteristics of the laser-melted Mg-Zn alloy are shown in Figure 2. It could be observed that the Mg-*x*Zn alloys consisted of the Mg matrix and a small amount of the second phase.

The average grain sizes of Mg-2Zn, Mg-4Zn, Mg-6Zn and Mg-8Zn were approximately 20 μm, 18 μm, 16 μm and 15 μm, respectively. It was concluded that the grain was refined as the Zn increased, while the effect of grain refinement decreased when the Zn content exceeded 6 wt. %. Nevertheless, the grain sizes of laser-melted Mg-Zn alloys were smaller than those of as-cast Mg alloys, with a typical size of 100 μm [21]. It was believed that second-phase particles pinning in the matrix hindered the growth of grains. On the other hand, the time for grain growth was very short due to rapid laser melting/solidification, which also contributed to limiting the growth of grains [22].
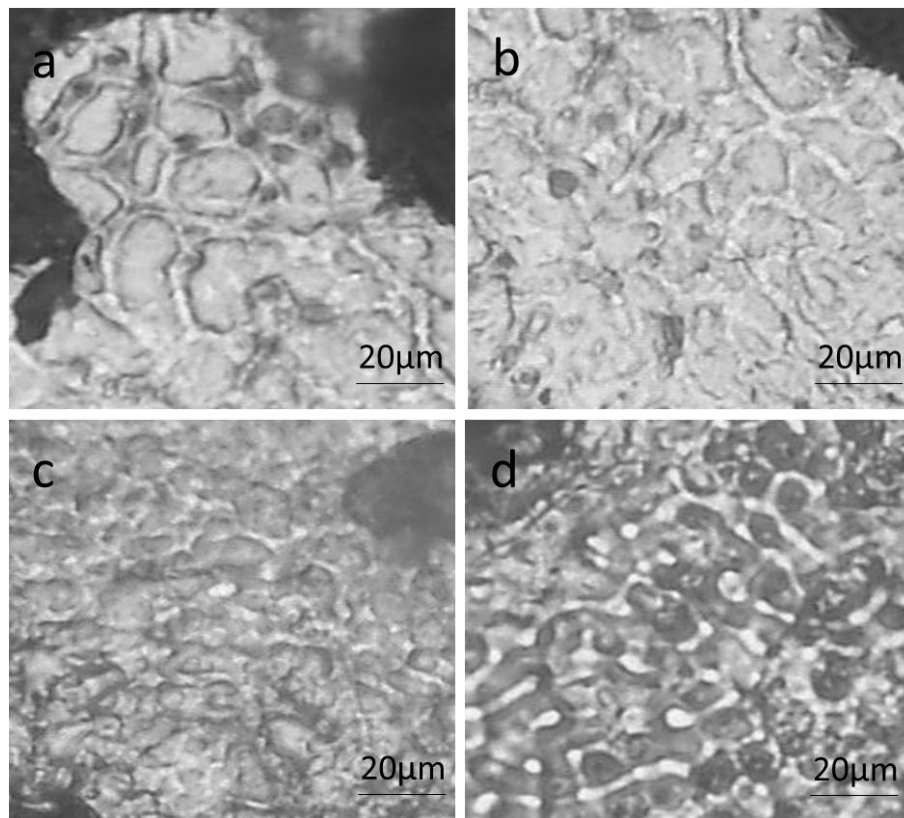

Figure 2. Optical microstructure of Mg-Zn alloys: (**a**) Mg-2Zn; (**b**) Mg-4Zn; (**c**) Mg-6Zn; and (**d**) Mg-8Zn.

The backscattered electron mode in the SEM was used to further investigate the size, volume percent, distribution, and shape of the secondary phases in the alloys. Owing to the different atomic number between Mg and Zn, the images clearly show that Mg-2Zn mainly contained the α-Mg phase (Figure 3a), while the Zn-rich second phase could be detected in Mg-6Zn and Mg-8Zn alloys (Figure 3c,d). As shown in Figure 3, the light area corresponds to the second phase. The dot-like second phase appeared along the grain boundary when the Zn content was not over 4%. In Mg-6Zn alloys, the second phase dispersed at the grain boundary, while it formed a reticular structure with the Zn content up to and over 8 wt. %. These results indicate that the size and volume percent in the second phase both increased as Zn increased. The microstructure of the etched alloy and the EDS analysis were shown in Figure 4. The results revealed that area B, which existed in the inner grain, was composed of 98.45 wt. % Mg and 1.55 wt. % Zn, whereas area A which existed in the grain boundary was composed of 66.59 wt. % Mg and 33.41 wt. % Zn. Thus, it was reasonable to conclude that the Zn-rich second phase distributed along the grain boundaries.
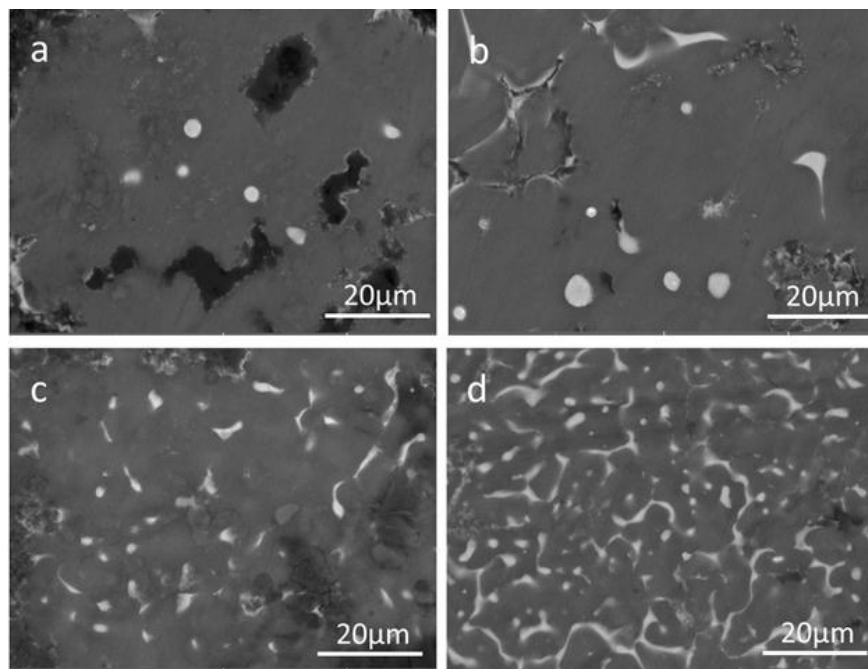
Figure 3. SEM micrograph of the Mg-Zn alloys: (**a**) Mg-2Zn; (**b**) Mg-4Zn; (**c**) Mg-6Zn and (**d**) Mg-8Zn.

Element	Wt%	At%
Mg	66.59	84.27
Zn	33.41	15.73

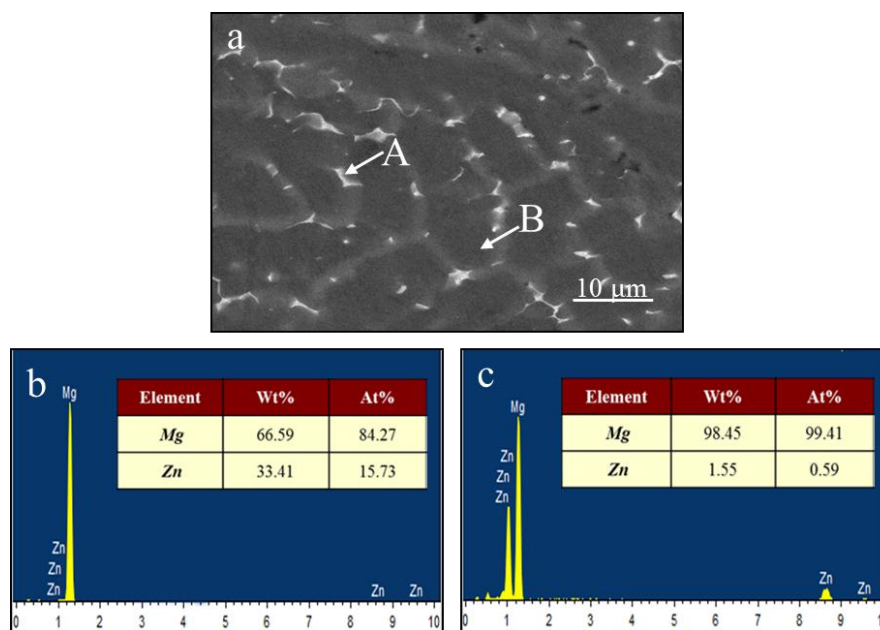| Element	Wt%	At%
Mg	98.45	99.41
Zn	1.55	0.59

Figure 4. (**a**) SEM of the etched Mg-Zn alloys; (**b**) EDS results of area A in Figure 4a and (**c**) EDS results of area B in Figure 4a.

XRD was used to analyze the phase composition of the Mg-Zn alloys (Figure 5). Strong α-Mg peaks were detected in Mg-xZn (x = 2, 4, 6 and 8 wt. %) alloys, while weak peaks corresponding to MgZn were clearly detected in Mg-6Zn and Mg-8Zn alloys. Furthermore, the peaks' intensity of MgZn phase became stronger as the Zn content increased (Table 2), implying that the volume percent of the MgZn phase increased. The peaks of MgZn were barely detectable in Mg-2Zn and Mg-4Zn, because the quantity of Zn was too small to be detected. This phenomenon also explains why there was little dot phase in Mg-2Zn and Mg-4Zn (Figure 3).
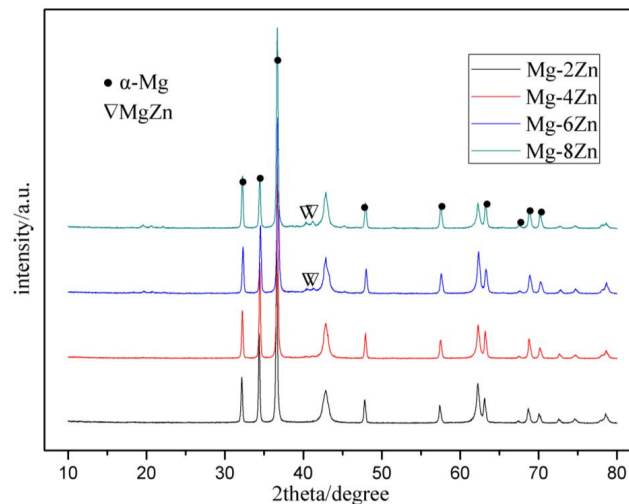
Figure 5. XRD patterns of laser-melted Mg-Zn alloys.

Table 2. The diffraction peak intensity of the MgZn phase in Mg-Zn alloys.

Sample	Mg-2Zn	Mg-4Zn	Mg-6Zn	Mg-8Zn
Intensity	320	400	455	486

3.2. Degradation Behavior

The relationship between the variation of the hydrogen volume and immersion time is shown in Figure 6. It was found that the evolved hydrogen volume rapidly increased during the initial three days, then slowed down and stabilized after five days. Besides, after immersion for seven days, the evolved hydrogen volume of Mg-6Zn (32.2 mL/cm^2) was lower than that of Mg-2Zn (47.1 mL/cm^2), Mg-4Zn (40.3 mL/cm^2) and Mg-8Zn (36.4 mL/cm^2).
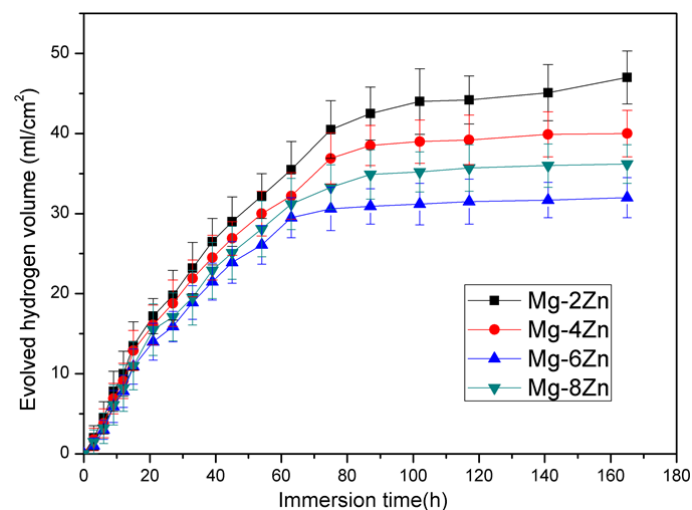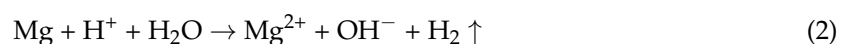

Figure 6. The evolved hydrogen volumes of the Mg-Zn alloys immersed in SBF.

The variation of the evolved hydrogen volume was believed to be related to the activity of Mg in aqueous solution. When Mg alloys were soaked in SBF, the following reaction occurred [23]:

$$Mg + H^+ + H_2O \rightarrow Mg^{2+} + OH^- + H_2 \uparrow \tag{2}$$

This reaction demonstrates that the corrosion of Mg accompanied the release of hydrogen. Thus, it was reasonable to conclude that Mg-6Zn exhibited an improved degradation behavior compared with Mg-2Zn, Mg-4Zn and Mg-8Zn. This improved degradation behavior could be ascribed to an enhanced corrosion potential with increasing Zn. Cai et al. [21] reported that the Zn element could increase the corrosion potential, thus improving corrosion resistance. Moreover, the high grain boundary density caused by grain refinement was also beneficial for the improvement of the degradation behavior. Wang et al. [24] studied the bio-corrosion behavior of Mg alloy AZ31 and verified that the degradation rate of this alloy after immersion in Hank's solution was significantly reduced due to grain refinement. However, the degradation rate accelerated when Zn content was further increased. It was believed that the second phase and impurities acted as effective galvanic cathodes coupled with the Mg matrix, and formed many anode-cathode sites, which resulted in micro-galvanic corrosion [25]. On the other hand, second phases and impurities were redistributed due to rapid cooling during laser melting, which reduced the adverse effect of nonequilibrium microstructures. Moreover, the grains were further refined after laser melting. Therefore, laser-melted Mg-Zn alloys exhibited more excellent degradation behaviors than Mg-Zn alloys prepared by traditional processing.

The typical surface morphology of Mg-6Zn after immersion in SBF is shown in Figure 7a. It could be observed that a large amount of corrosion product formed on the surface. Corresponding EDS results revealed that the corrosion product consisted of Mg, oxygen (O), Zn and chlorine (Cl) (Figure 7b). XRD was performed to further identify the phase composition of the corrosion product. Results revealed that the product was mainly composed of $Mg(OH)_2$. Similar results were obtained in the study by Zhang [13], in which the corrosion layer of the Mg-Zn alloy contained $Mg(OH)_2$, HA and some Mg-substituted apatite. A large amount of $Mg(OH)_2$ was coated on the surface of the alloy as Mg alloys were soaked in SBF, which formed a protective layer [26]. Thus, the degradation rate slowed down during the late period of immersion (Figure 7).
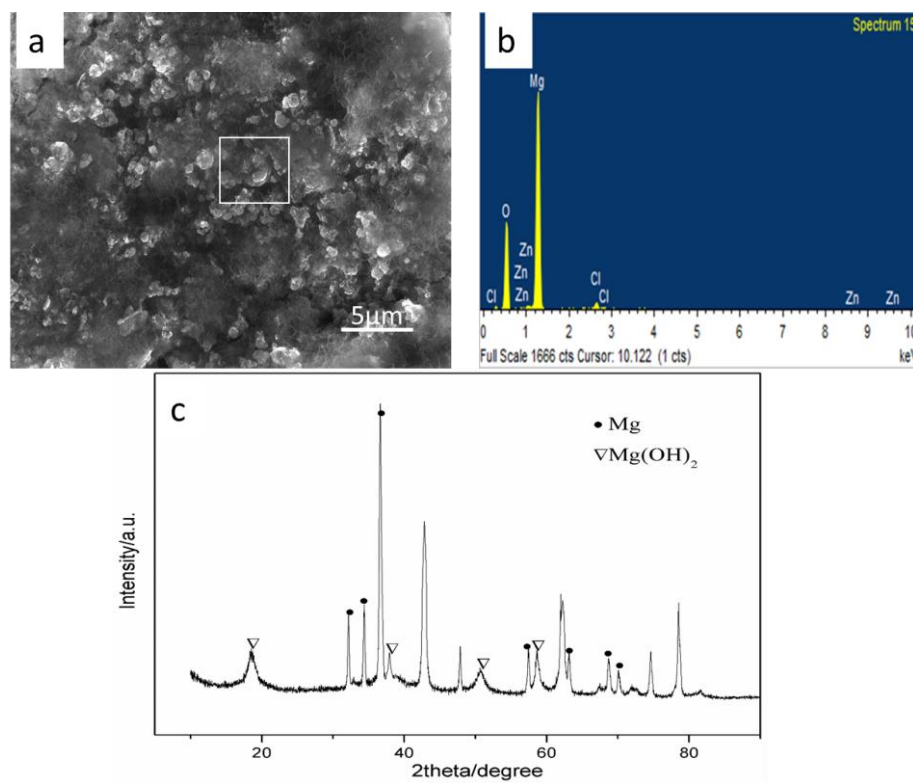

Figure 7. Corrosion products of the Mg-6Zn in SBF: (**a**) surface morphology; (**b**) composition analysis of EDS; (**c**) XRD identification.

3.3. Mechanical Properties

The relationship between the hardness of the alloys and Zn content was studied, as shown in Figure 8. Hardness constantly increased as the Zn content was increased. Hardness increased from 62 ± 0.05 Hv to 71.5 ± 0.05 Hv when the Zn content was increased from 2 to 8 wt. %. Nevertheless, the hardness of laser-melted Mg-Zn alloys was considerably higher than that of the selective laser-melted pure Mg with an average hardness of 45 Hv [19]. Hardness is an important mechanical property to estimate whether materials, especially alloys, can be used for bone implants [27]. It has been well recognized that mechanical properties are influenced by numerous factors, such as phase distribution, grain size, grain boundary conditions, and defects. Given that, the improvement of mechanical properties was attributed to the fact that MgZn phases precipitated from the Mg matrix and acted as a reinforcement phase. The MgZn phase served as the hard particle, gradually increasing the hardness as the size of the MgZn phase increased. Moreover, the dispersion strengthening effect caused by the homogenously distributed MgZn phases enhanced with the increase of the second phase volume fraction [28]. On the other hand, the grain refinement caused by the presence of the Mg-Zn phase and rapid solidification was also beneficial to the improvement of mechanical properties, especially for hexagonal close-packed Mg [29]. Grain boundaries were the effective barriers of grain boundary sliding. With grain refining, several grain boundary slip systems were activated and caused uniform deformation, leading to improved hardness.
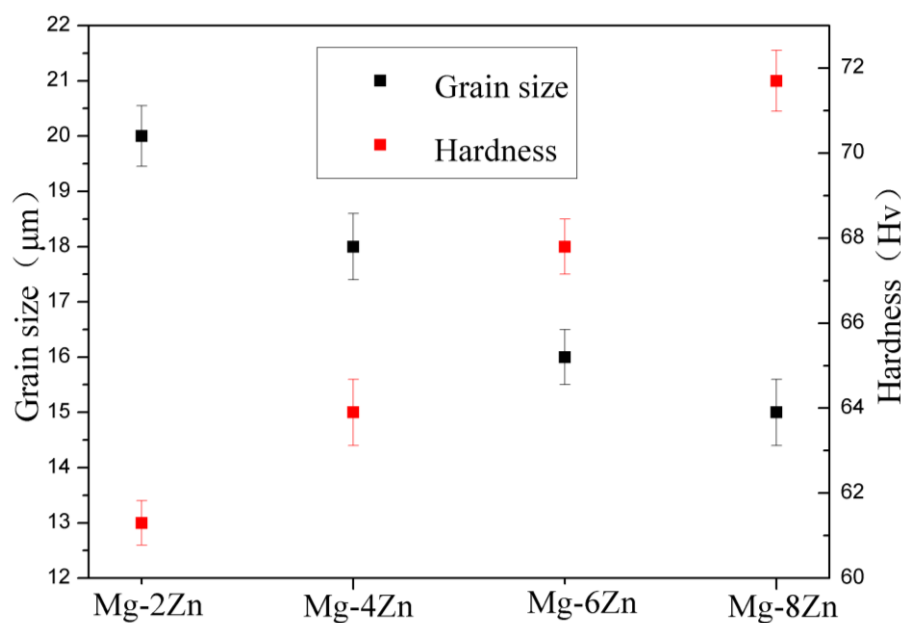

Figure 8. The grain size and hardness of the Mg-Zn alloys.

4. Conclusions

In this study, Mg-Zn alloys were prepared by laser melting. The grain was refined after alloying Zn and laser melting due to the inhibiting effect of the MgZn phase on grain growth and rapid solidification. The refining effect decreased when the Zn content was over 6 wt. %. These degradation rates gradually slowed down as the Zn content increased to 6 wt. %, due to grain refinement and increased corrosion potential. Mg-6Zn has been proven to possess the optimal degradation behavior. The hardness of the Mg-Zn alloys increased from 62 ± 0.05 Hv to 71.5 ± 0.05 Hv. Taking into the consideration both degradation behavior and mechanical properties, Mg-Zn alloys fabricated by laser melting are potential candidates for biomaterials.

Author Contributions: C.S. and Y.D. conceived and designed the experiments; J.C. performed the experiments; Y.Z. and Y.Y. analyzed the data; P.W., S.P. contributed reagents/materials/analysis tools; J.C. wrote the paper.

Conflicts of Interest: The authors declare no conflict of interest.

References

1. Jamesh, M.; Wu, G.S.; Zhao, Y.; Chu, P.K. Electrochemical corrosion behavior of biodegradable Mg-Y-RE and Mg-Zn-Zr alloys in Ringer's solution and simulated body fluid. *Corros. Sci.* **2013**, *69*, 158–163. [CrossRef]

2. Chou, D.; Hong, D.; Saha, P.; Ferrero, J.; Lee, B.; Tan, Z.Q.; Dong, Z.Y.; Kumt, P.N. In vitro and in vivo corrosion, cytocompatibility and mechanical properties of biodegradable Mg-Y-Ca-Zr alloys as implant materials. *Acta Biomater.* **2013**, *9*, 8518–8533. [CrossRef] [PubMed]

3. Seitz, J.M.; Eifler, R.; Bach, F.W.; Maier, H.J. Magnesium degradation products: Effects on tissue and human metabolism. *J. Biomed. Mater. Res. A* **2014**, *102*, 3744–3753. [CrossRef] [PubMed]

4. Tie, D.; Guan, R.; Liu, H.; Cipriano, A.; Liu, Y.; Wang, Q.; Huang, Y.; Hort, N. An in vivo study on the metabolism and osteogenic activity of bioabsorbable Mg-1Sr alloy. *Acta Biomater.* **2016**, *29*, 455–467. [CrossRef] [PubMed]

5. Chaya, A.; Yoshizawa, S.; Verdelis, K.; Myers, N.; Costello, B.J.; Chou, D.; Pal, S.; Maiti, S.; Kumta, P.N.; Sfeir, C. In vivo study of magnesium plate and screw degradation and bone fracture healing. *Acta Biomater.* **2015**, *18*, 262–269. [CrossRef] [PubMed]

6. Zheng, Y.F.; Gu, X.N.; Witte, F. Biodegradable metals. *Mater. Sci. Eng. R Rep.* **2014**, *77*, 1–34. [CrossRef]

7. Hampp, C.; Angrisani, N.; Reifenrath, J. Evaluation of the biocompatibility of two magnesium alloys as degradable implant materials in comparison to titanium as non-resorbable material in the rabbit. *Mater. Sci. Eng. C* **2013**, *33*, 317–326. [CrossRef] [PubMed]

8. Ding, Y.; Wen, C.; Hodgson, P.; Li, Y. Effects of alloying elements on the corrosion behavior and biocompatibility of biodegradable magnesium alloys: A review. *J. Mater. Chem. B* **2014**, *2*, 1912–1933. [CrossRef]

9. Cao, F.; Shi, Z.; Song, G.L. Effect of alloying elements on corrosion behaviour of binary magnesium alloys. In Proceedings of the Annual Conference Proceedings: Australasian Corrosion Association, Brisbane, Australia, 10–13 November 2013; pp. 1–12.

10. Esmaily, M.; Navid, M.S.; Mortazavib, N.; Svensson, J.E.; Halvarsson, M.; Wessén, M.; Jarfors, A.E.W.; Johansson, L.G. Microstructural characterization of the Mg-Al alloy AM50 produced by a newly developed rheo-casting process. *Mater. Charact.* **2014**, *95*, 50–64. [CrossRef]

11. Qiao, Y.; Zhang, W.; Tian, P.; Meng, F.; Zhu, H.; Jiang, X.; Liu, X.; Chu, P.K. Stimulation of bone growth following zinc incorporation into biomaterials. *Biomaterials* **2014**, *35*, 6882–6897. [CrossRef] [PubMed]

12. Boehlert, C.J.; Knittel, K. The microstructure, tensile properties, and creep behavior of Mg-Zn alloys containing 0–4.4 wt. % Zn. *Mater. Sci. Eng. A* **2006**, *417*, 315–321. [CrossRef]

13. Zhang, X.; Xie, C.; Zhang, Y.; Tao, H.; He, Y.; Jiang, Y. In vitro degradation, hemolysis and MC3T3-E1 cell adhesion of biodegradable Mg-Zn alloy. *Mater. Sci. Eng. C* **2009**, *29*, 1907–1912. [CrossRef]

14. Song, B.; Zhao, X.; Li, S.; Han, C.; Wei, Q.; Wen, S.; Shi, Y. Differences in microstructure and properties between selective laser melting and traditional manufacturing for fabrication of metal parts: A review. *Front. Mech. Eng.* **2015**, *10*, 111–125. [CrossRef]

15. Ng, C.C.; Savalani, M.M.; Lau, M.L. Microstructure and mechanical properties of selective laser melted magnesium. *Appl. Surf. Sci.* **2011**, *257*, 7447–7454. [CrossRef]

16. Yadroitsev, I.; Krakhmalev, P.; Yadroitsava, I. Selective laser melting of Ti6Al4V alloy for biomedical applications: Temperature monitoring and microstructural evolution. *J. Alloys Compd.* **2014**, *583*, 404–409. [CrossRef]

17. Shahzad, M.; Waqas, H.; Qureshi, A.H.; Wagner, L. The roles of Zn distribution and eutectic particles on microstructure development during extrusion and anisotropic mechanical properties in a Mg-Zn-Zr alloy. *Mater. Sci. Eng. A* **2015**, *620*, 50–57. [CrossRef]

18. McKeown, J.T.; Zweiacker, K.; Liu, C.; Coughlin, D.R.; Clarke, A.J.; Baldwin, J.K.; Gibbs, J.W.; Roehling, J.D.; Imhoff, S.D.; Gibbs, P.J. Time-Resolved In Situ Measurements During Rapid Alloy Solidification: Experimental Insight for Additive Manufacturing. *JOM* **2016**, *68*, 985–999. [CrossRef]

19. Yang, Y.; Wu, P.; Lin, X.; Liu, Y.; Bian, H.; Zhou, Y.; Shuai, C. System development, formability quality and microstructure evolution of selective laser-melted magnesium. *Virtual Phys. Prototyp.* **2016**, *11*, 173–181. [CrossRef]

20. Freni, A.; Dawoud, B.; Bonaccorsi, L.; Chmielewski, S.; Frazzica, A.; Calabrese, L.; Restuccia, G. *Characterization of Zeolite-Based Coatings for Adsorption Heat Pumps*; Springer: Messina, Italy, 2015; p. 81.

21. Cai, S.; Lei, T.; Li, N.; Feng, F. Effects of Zn on microstructure, mechanical properties and corrosion behavior of Mg-Zn alloys. *Mater. Sci. Eng. C* **2012**, *32*, 2570–2577. [CrossRef]

22. Vrancken, B.; Thijs, L.; Kruth, J.P. Microstructure and mechanical properties of a novel β titanium metallic composite by selective laser melting. *Acta Mater.* **2014**, *68*, 150–158. [CrossRef]

23. Wang, Y.; Wei, M.; Gao, J.; Hu, J.; Zhang, Y. Corrosion process of pure magnesium in simulated body fluid. *Mater. Lett.* **2008**, *62*, 2181–2184. [CrossRef]

24. Wang, H.; Estrin, Y.; Fu, H.M.; Song, G.L.; Zuberova, Z. The effect of pre-processing and grain structure on the bio-corrosion and fatigue resistance of magnesium alloy AZ31. *Adv. Eng. Mater.* **2007**, *9*, 967–972. [CrossRef]

25. Song, Y.; Shan, D.; Chen, R. Effect of second phases on the corrosion behaviour of wrought Mg-Zn-Y-Zr alloy. *Corros. Sci.* **2010**, *52*, 1830–1837. [CrossRef]

26. Rad, H.R.B.; Hamzah, E.; Lotfabadi, A.F. Microstructure and bio-corrosion behavior of Mg-Zn and Mg-Zn-Ca alloys for biomedical applications. *Mater. Corros.* **2014**, *65*, 1178–1187.

27. Hodgskinson, R.; Currey, J.D.; Evans, G.P. Hardness, an indicator of the mechanical competence of cancellous bone. *J. Orthop. Res.* **1989**, *7*, 754–758. [CrossRef] [PubMed]

28. Lv, B.; Peng, J.; Peng, Y. The effect of addition of Nd and Ce on the microstructure and mechanical properties of ZM21 Mg alloy. *J. Magnes. Alloy.* **2013**, *1*, 94–100. [CrossRef]

29. Okuda, H.; Horiuchi, T.; Tsukamoto, T.; Ochiai, S.; Yamasaki, M.; Kawamura, Y. Evolution of long-period stacking ordered structures on annealing as-cast $Mg_{85}Y_9Zn_6$ alloy ingot observed by synchrotron radiation small-angle scattering. *Scr. Mater.* **2013**, *68*, 575–578. [CrossRef]